Performance of Two-Equation Turbulence Models for Flat Plate Flows With Leading Edge Bubbles

S. Collie

M. Gerritsen

P. Jackson

Stanford Yacht Research,
367 Panama Street,
Stanford, CA 94305-2220

This paper investigates the performance of the popular k-ω and SST turbulence models for the two-dimensional flow past the flat plate at shallow angles of incidence. Particular interest is paid to the leading edge bubble that forms as the flow separates from the sharp leading edge. This type of leading edge bubble is most commonly found in flows past thin airfoils, such as turbine blades, membrane wings, and yacht sails. Validation is carried out through a comparison to wind tunnel results compiled by Crompton (2001, "The Thin Aerofoil Leading Edge Bubble," Ph.D. thesis, University of Bristol). This flow problem presents a new and demanding test case for turbulence models. The models were found to capture the leading edge bubble well with the Shear-Stress Transport (SST) model predicting the reattachment length within 7% of the experimental values. Downstream of reattachment both models predicted a slower boundary layer recovery than the experimental results. Overall, despite their simplicity, these two-equation models do a surprisingly good job for this demanding test case. [DOI: 10.1115/1.2829596]

Keywords: turbulence, leading edge bubble, computational fluid dynamics

1 Introduction

In this study, we investigate the performance of the SST and k-ω turbulence models for thin leading edge bubbles of the type found in the flow past flat plates at shallow incidence. The numerical results are compared with the high-quality wind tunnel data obtained by Crompton [1]. The wind tunnel data allow for an accurate validation of simulation results. The test case is unique and poses a challenging assignment for two-equation turbulence models. The notable features of the flow field are unsteady shear layer flapping, shear layer transition, relaminarization, secondary recirculation, flow reattachment, and postreattachment boundary layer recovery. Each of these flow features directly challenges the assumptions from which many turbulence models are derived. The current investigation focusses on two-equation turbulence models that are generally viewed as the most practical models for industrial engineering applications. Of these models the k-ω and Shear-Stress Transport (SST) models are considered amongst the best for flows involving separation [2]. A preliminary Large Eddy Simulation (LES) study is also conducted and reported in the discussion section.

Both Crompton's study and this work were motivated by the desire to improve physical understanding and simulation of flows past yacht sails. The thin airfoil bubbles investigated here will usually exist for sails that are not supported by a mast (i.e., headsails such as genoas and jibs, or downwind sails such as spinnakers and gennakers). The bubbles significantly influence the pressure distribution and lift generated by such sails. The flexible nature of such sails is an important design consideration. Aeroelastic studies are ultimately needed to create the design that produces the desired flying shape. However, the nature of flows past downwind sails is not yet well understood, and the first question that must be answered is what sail shape provides the best aerodynamic performance. This work contributes to improving our understanding of downwind sail flows [3]. Thin airfoil bubbles occur in many other flows, such as flows past thin airfoils and membrane wings, and therefore this work is also of direct interest to a much wider range of fluid flow problems than those in the sailing community.

2 Flow Past Flat Plate at Shallow Incidence

2.1 Flow Structure. A schematic of the flow past the flat plate is provided in Fig. 1. This flow structure was first described in the experimental work of Gault [4] where he described the bubble as being vastly different from leading edge bubbles typically found on airfoils. The shear layer that separates from the leading edge is immediately unstable. Vortices are shed periodically from the tip of the plate and advected along the shear layer. Driver et al. [5] observed a similar vortex shedding in the mixing layer behind a backward facing step and referred to the phenomenon as shear layer flapping. Both the backward facing step flow of Driver et al. and the flow past the flat plate at shallow incidence involve a turbulent shear layer that separates from a point and reattaches some distance downstream. For the backward facing step of Driver et al., the performance of k-ε models have been shown to give poor results compared with the k-ω and SST models [6,7].

In Crompton's experiments, the separated shear layer was found to undergo transition within the first 2.5% of the length of the plate. Downstream of transition, turbulent kinetic energy is entrained rapidly due to high mean shear across the shear layer. This entrainment of turbulent kinetic energy causes the shear layer to thicken and curve back toward the surface of the plate. As the shear layer approaches the surface of the plate, the velocity fluctuations in the direction normal to the plate are damped. Energy from the normal fluctuations is converted to the other components of the Reynold stress tensor, with the turbulent eddies stretching in the spanwise and streamwise directions. The flow reattaches some distance, X_R, downstream of the leading edge. Here, the flow bifurcates with the bulk of the flow continuing along the length of the plate, while a smaller fraction is driven back toward the leading edge to complete the leading edge bubble. The boundary layer that forms downstream of the reattachment point is embedded with turbulent structures that are a legacy from the leading edge bubble. These mixing layer structures advect downstream

Contributed by the Fluids Engineering Division of ASME for publication in the JOURNAL OF FLUIDS ENGINEERING. Manuscript received June 6, 2005; final manuscript received July 26, 2007; published online January 24, 2008. Review conducted by Surya P. Vanka.

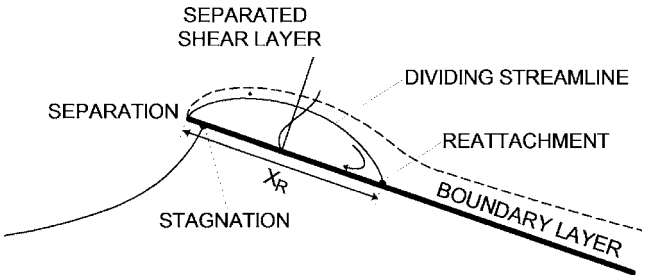

Fig. 1 Schematic of the flow past a flat plate at shallow incidence

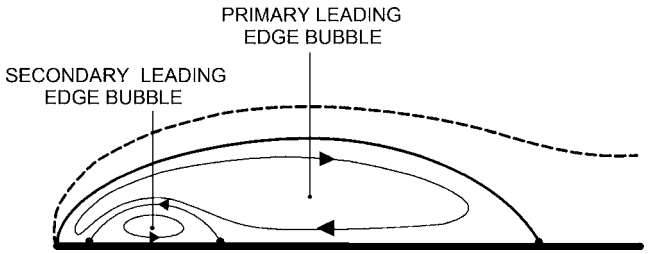

Fig. 2 Schematic of the leading edge bubble illustrating the secondary bubble near the leading edge

and interact with the development of the boundary layer.

The recovering turbulent boundary layer has a unique structure that is atypical of turbulent boundary layers; it is sluggish and prone to boundary layer separation in adverse pressure gradient flows. Naturally, the structure of the boundary layer during recovery dictates the size and structure of any trailing edge separation region that might form downstream. Consequently, the nature of the boundary layer after reattachment can have a significant impact on the lift coefficient. Naturally, the shape and structure of the separation region itself affect the pressure peak near the leading edge, which is the primary contributor to lift. The interaction between the leading edge bubble and the trailing edge separation region is as yet not fully understood.

The type of leading edge bubble found on the flat plate at shallow incidence is also known as the thin airfoil bubble. It should not be confused with the short bubble, or laminar separation bubble, which often appears on low Reynolds number airfoils due to laminar separation near the nose [8]. The primary difference between the two bubble types is that the shear layer in the thin airfoil bubble is predominantly turbulent, whereas the shear layer in the short bubble is typically laminar over more than half the length of the bubble. The difference here is that the laminar bubble separates due to the presence of an adverse pressure gradient, whereas the thin airfoil bubble is forced to separate abruptly as the flow rounds the leading edge.

2.2 Experimental Data. Of the experimental results concerned with the flat plate at shallow incidence, the thesis by Crompton [1] is the most comprehensive. Crompton presents a detailed examination of the bubble structure, which extends upon earlier work by Gault [4] and Newman and Tse [9]. The blunt plate experimental studies of Cherry et al. [10] as well as Kiya and Sasaki [11] also provide insight to separated and reattaching flows. However, these flows involve large scale unsteadiness due to the blunt rectangular shaped leading edge. Due to this difference in leading edge geometry, such flows are less suitable for the validation of sail flow simulations compared with the Crompton data.

Through the use of laser Doppler anemometry (LDA), Crompton was able to obtain accurate measurements of the velocity and turbulence statistics for the leading edge bubble. LDA measurements of the developing turbulent boundary layer in the recovery region downstream of the reattachment point were also taken. Surface pressures were recorded through static pressure tappings. Flow visualization techniques (surface tufts, china clay, and oil streakline) were used to complement the LDA and static pressure data. Unfortunately, no skin friction measurements were conducted in the experiments.

In his experiments, Crompton detected a secondary separation bubble very close to the leading edge of the plate, which had not been witnessed in previous studies (see Fig. 2). The secondary bubble is created as the reversed flow within the leading edge bubble separates due to the adverse pressure gradient that exists over the forward half of the bubble. The reversed flow is particularly prone to separate due to relaminarization of the reversed flow [1].

The wind tunnel model used in Crompton's experiments had a chord length of 160 mm and a span of 800 mm, giving an aspect ratio of 5, which was demonstrated (using oil-streakline flow visualization) to be sufficient to provide nominally two-dimensional flow [1]. The plate was constructed out of a 6 mm steel plate, giving a thickness to chord ratio of 3.75%. This thickness provided enough stiffness to minimize deflection and also facilitated the use of pressure tappings. The leading edge of the plate was chamfered at 20 deg to provide the sharp leading edge required for knife edge separation to occur exactly at the tip of the plate. A cross section of the model is illustrated in Fig. 3.

Crompton's experiments were carried out over a range of Reynolds numbers $(0.1\times10^5-5.5\times10^5)$ to investigate Reynolds number dependency. The reattachment length was found to be independent of Reynolds number above 10^5. Also, the Reynolds number was not found to have an influence on the flow downstream of the reattachment point (because of the turbulent reattachment process).

The primary wind tunnel investigation was performed at a Reynolds number of 2.13×10^5, and it is at this Reynolds number that a comparison between the experiments and computational fluid dynamics (CFD) have been made. The experimental data are provided for angles of attack, $\alpha=1-5$ deg, in 1 deg intervals. At $\alpha=1$ deg, the leading edge bubble is small and similar in length to chord ratio to leading edge bubbles observed for downwind sail flows in the University of Auckland's twisted flow wind tunnel [3]. At $\alpha=5$ deg, the flow is separated for most of the plate, and at $\alpha=6$ deg, the shear layer fails to reattach. The asymmetry of the plate creates a lift force even at zero degrees of incidence, which causes the flow to curve upward (in the direction of the lift axis) near the leading edge of the plate; consequently, a small leading edge separation bubble forms at zero angle of attack. The so-called "ideal" angle of incidence, where laminar boundary layers are able to develop on both surfaces without leading edge separation, occurs at a small negative angle.

3 Computational Fluid Dynamics Model

3.1 Turbulence Models and Numerical Solvers. The software used in this study is CFX-5, an unstructured commercial CFD package [12]. In the CFX-5 solver, the Reynolds Averaged Navier-Stokes Equations (RANS) equations are discretized using a conservative and time-implicit finite volume method and are solved using an additive correction algebraic multigrid (AMG) solver, accelerated with an incomplete lower upper (ILU) factorization technique. Details of these techniques and their implementation can be found in Refs. [12,13]. Spatial interpolation is carried out using the second-order upwind advection scheme, details

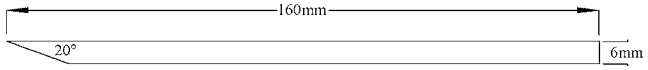

Fig. 3 Model dimensions

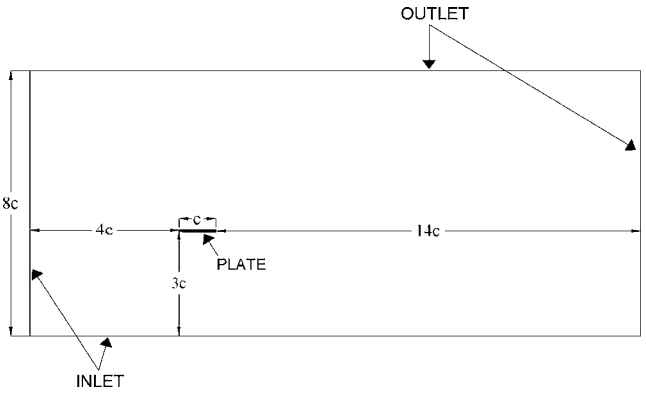

Fig. 4 Details of the domain for the flat plate

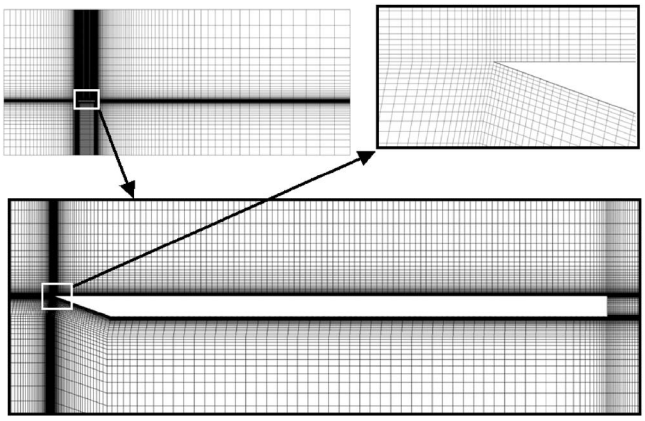

Fig. 5 Computational grid for the flat plate (medium resolution)

of which can be found in Ref. [12]. The simulations were carried out using the SST [14] and standard k-ω [15] turbulence models and all simulations converged to a steady state with all residuals decreasing by at least four orders of magnitude. Crompton [1] reported evidence of shear layer unsteadiness at the leading edge. However, in this CFD, no evidence of unsteadiness was found, even when very small time steps were used.

Simulations were also carried out using the standard k-ε model for comparative purposes. However, it was found that the algebraic wall functions used to capture the inner portion of the boundary layer in these models do not perform well for this flat plate flow. The wall functions assume that the inner boundary layer region is in turbulent equilibrium, which is not the case here, especially within the leading edge bubble. The k-ε model was found to diverge for the fine grids that were used in this study, and convergence was obtained only on grids much coarser than desired. Consequently, only results computed using the k-ω and SST models are presented in this paper.

3.2 Computational Domain and Gridding. Crompton's flat plate was modeled using the same geometry as in the experiments (Fig. 3). The computational domain is illustrated in Fig. 4. Simulations performed using a domain twice the size verified that the domain dimensions of Fig. 4 were adequate in that the proximity of the far-field boundaries did not affect the near field. At the inlet, Cartesian velocity components were specified according to the angle of incidence. The freestream turbulence intensity was set at 0.05%, which was the maximum value measured during the wind tunnel experiments [1]. The turbulent length scale was set at $0.001m$, a typical value for low turbulence wind tunnels. At the outlet, the static pressure is set at zero, and a constant gradient constraint is imposed on turbulence quantities.

Block-structured grids were generated in ICEM-HEXA [16]. Three grid resolutions were used. We refer to the grids as coarse, medium, and fine with 11,920, 49,625, and 202,435 cells, respectively. The medium and fine grids were constructed from the coarse and medium grids, respectively, by grid halving in both directions. A grid convergence study is presented in Sec. 4.1. The medium grid is illustrated in Fig. 5. In order to achieve a y^+ of around 1.0, the near-wall spacing was set at 1.0×10^{-5} m. Particular care was taken to provide high quality cells around the leading edge. The grid cells have an aspect ratio of 1:1 at the tip. The tip region is illustrated in the close-up view in Fig. 5. Along the plate, the aspect ratio of the near-wall cells is gradually increased to take advantage of the relatively small flow gradients tangential to the wall compared with those in the wall normal direction. The maximum cell aspect ratio, which occurs at the trailing edge, is set at 1:10.

4 Results

This section initially focuses on the case at $\alpha=1$ deg, for which the flow is most similar to flows past downwind sails. At this angle, the leading edge separation bubble stretches across the first 14% of the chord length (i.e., $X_R/c=0.14$), which is approximately the same as for downwind sail flows. Since the bubble at this angle is small, fewer velocity measurements were taken within the bubble at this angle than at the higher angles of attack. Therefore, we also investigated the case of $\alpha=3$ deg in order to gain a better understanding of the flow within the separation bubble. For $\alpha=3$ deg, the reattachment length $X_R/c=0.47$, which shows that the flow is separated over almost half of the plate. For $\alpha=5$ deg, the flow is almost fully separated and does not have a recovery region. We have therefore left this case out of the main discussion and refer to it only briefly when comparing the accuracy of the turbulence models in predictions of the reattachment length (Sec. 4.2).

4.1 Grid Convergence Study. A grid convergence study was performed at $\alpha=3$ deg with the SST turbulence model. At $\alpha=1$ deg the results are not as grid dependent since there the flow separation is much less severe than at $\alpha=3$ deg. Lift and drag coefficients are presented in Fig. 6 for the sequence of grids. The force coefficients are plotted against $1/N$, a nondimensional measure of the grid spacing, with N^2 as the total number of cells in the grid.

The lift and drag coefficients converge as the grid is refined. The lift from the medium grid solution is within 0.015% of the fine grid solution and the drag is within 0.0055%. Subsequent refinement is unlikely to result in improved accuracy of the solution; therefore, the medium grid was used for the simulations reported in the remainder of this paper.

4.2 Reattachment Lengths. Figure 7 presents the reattachment length data for each angle of attack (1–5 deg). At low angles of attack, the SST model captures the reattachment length accurately. However, at larger angles, it underpredicts the reattachment length. In contrast, the k-ω model consistently overpredicts the length of the leading edge bubble. The reasons and consequences of this are discussed in Secs. 4.3 and 4.4.

4.3 Comparison at $\alpha=1$ deg

4.3.1 Boundary Layer Profiles in the Leading Edge Bubble. Boundary layer velocity profiles were measured by Crompton at nine different chordwise locations along the plate using LDA. The measurement stations are located at $x/c=\{0.031, 0.125, 0.25, 0.375, 0.5, 0.625, 0.75, 0.875, 1.0\}$. Figure 8 shows the position of these measurement stations in relation to the flow field at α

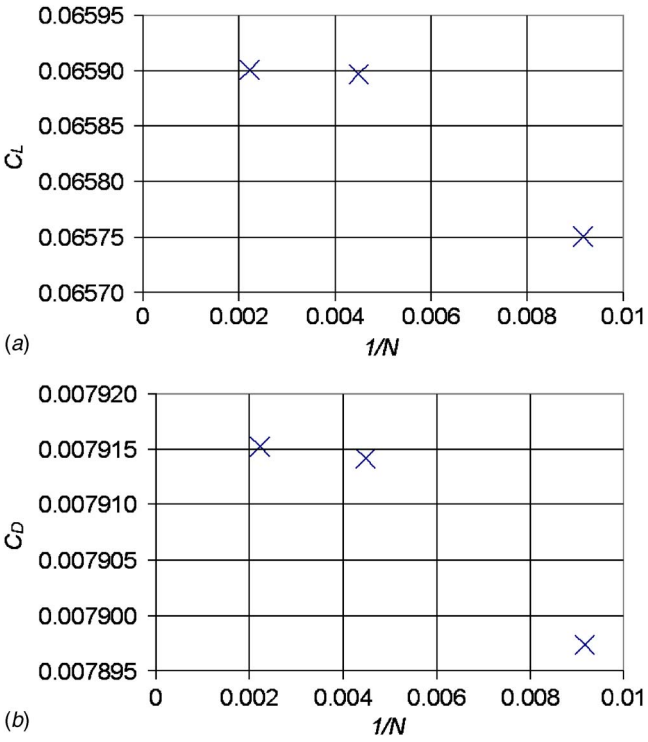

Fig. 6 Grid convergence of the lift and drag coefficients (α =3 deg)

=1 deg.

Table 1 shows that the reattachment lengths computed with the SST and k-ω models differ from the experimental values. The SST model overpredicts X_R by 5.8% and the k-ω model overpredicts X_R by 24.0%. To allow a better comparison between the boundary layer profiles, the measurement stations are scaled by X_R so that each station is in the same position relative to the reattachment point. For α=1 deg only the first two measurement stations are within the leading edge bubble. The profiles at these stations are shown in Fig. 9.

Table 1 Reattachment lengths for the flat plate at α=1 deg

	X_R
Crompton	0.14
SST	0.1486
k-ω	0.1841

The portion of the fluid forced upstream at the reattachment point is accelerated by the favorable pressure gradient and forms a reversed boundary layer. Crompton reported a maximum reversed velocity of $-0.4U_\infty$, approximately midway along the bubble. The CFD results show lower reversed velocities at the same position along the bubble, with the SST model predicting $-0.290U_\infty$ and the k-ω model predicting $-0.284U_\infty$. The measured velocities within the leading edge bubble are larger than usually experienced within short airfoil bubbles, for which the reversed flow velocity is typically below $-0.2U_\infty$ [1]. For the thin airfoil bubble, however, early transition results in a high rate of entrainment of turbulent kinetic into the bubble. Subsequently, greater velocities in both the outer and inner shear layers are observed. The turbulence models underpredict the entrainment rate and hence also underpredict the velocity magnitude throughout the leading edge bubble. This will be discussed further in Sec. 4.4, where the kinetic energy profiles within the separation bubble are presented.

Crompton reported that the reversed flow within the leading edge bubble experienced relaminarization, encouraged by the strong favorable pressure gradient, and that the inner shear layer began to show very laminarlike features. The velocity profiles within the separation bubble are presented in greater detail in Fig. 10. At x/c=0.031, in particular, the experimental data show a much more laminar profile than those provided by the CFD. To

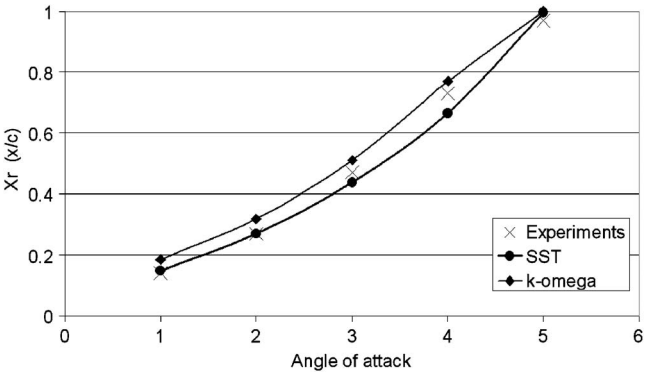

Fig. 7 Reattachment lengths versus angle of attack for the CFD compared with Crompton's data

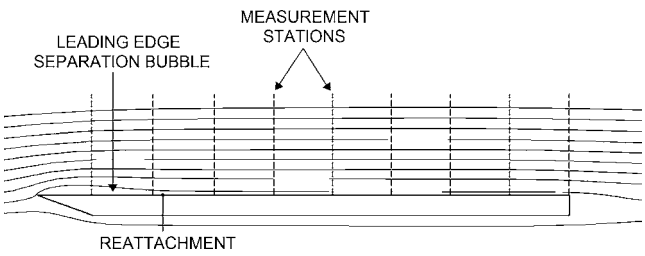

Fig. 8 Flow streamlines and the measurement stations for the flate plate at α=1 deg (SST model)

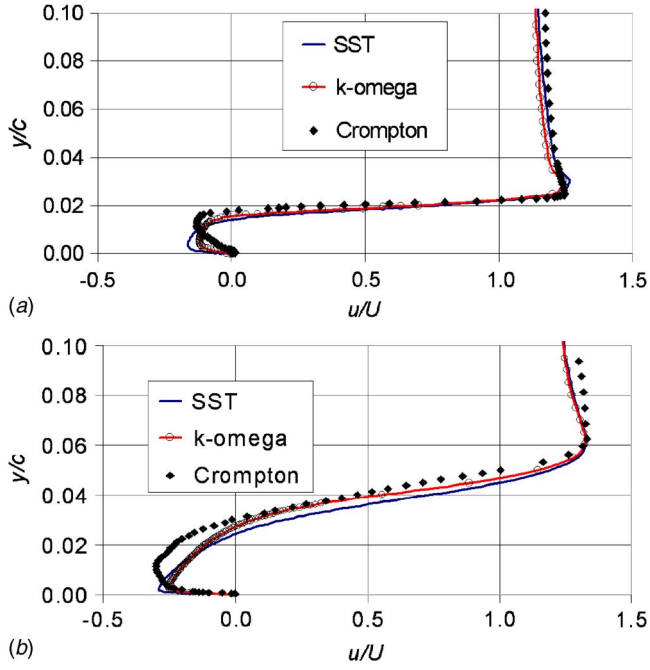

Fig. 9 Chordwise velocity profiles within the leading edge bubble (α=1 deg). (a) x/c=0.031, (b) x/c=0.125.

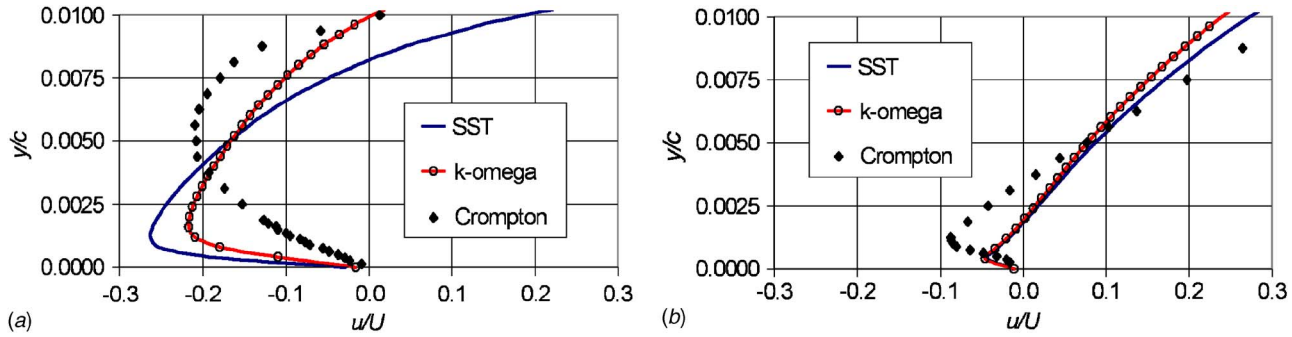

Fig. 10 Near-wall chordwise velocity profiles within the leading edge bubble (α=1 deg). (a) x/c=0.031, (b) x/c=0.125.

emulate the relaminarization process, an appropriate transition model is required, which is not provided by the turbulence models investigated.

One of the direct consequences of the more turbulentlike boundary layer profiles given by the CFD is their resistance to separation. In the simulations, the reversed boundary layer remains attached all the way to the leading edge, and there is no secondary separation of the type reported by Crompton. Crompton suggested that the form of this second bubble has significant influence on the development of the shear layer near the leading edge; consequently, its influence is likely to spread well downstream [1].

4.3.2 Boundary Layer Profiles Downstream of Reattachment. In Fig. 11, the boundary layer profiles at x/c=0.25 and 0.875 are presented using a log scale for y^+. Also plotted is a typical turbulent boundary layer at zero pressure gradient (ZPG) [17]. The wall shear stress τ_w was not provided in the experimental results; therefore, it was difficult to nondimensionalize the Crompton data. Here, y^+ and u^+ are calculated based on the τ_w values from the CFD data computed using the SST model. Any errors introduced by this approximation are likely to be small. The nondimensionalized plots in Fig. 11 follow the same trends as data compared using the raw velocity, U, and normal distance, y.

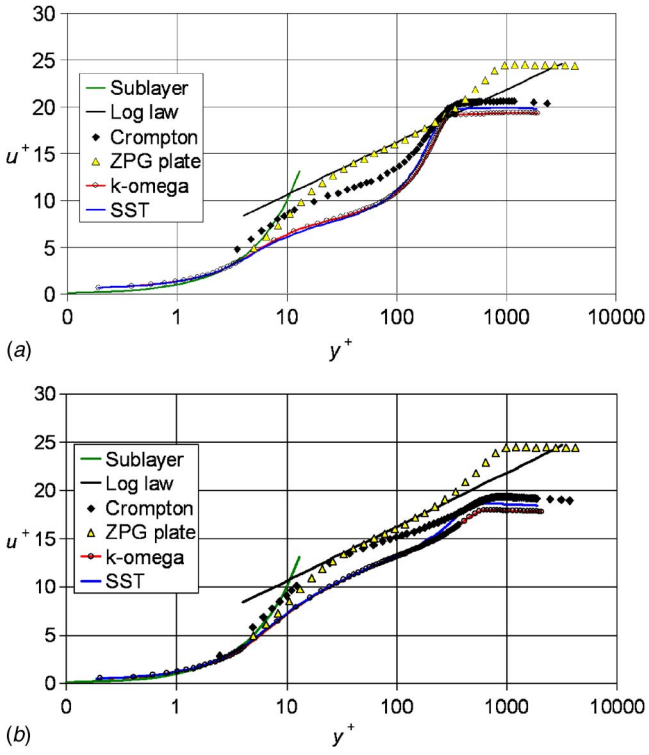

Fig. 11 Chordwise velocity profiles downstream of reattachment (log scale, α=1 deg). (a) x/c=0.250, (b) x/c=0.875.

At x/c=0.25, the boundary layer profiles given by the experiments and the CFD lie below the ZPG profile. This is expected because of the slight adverse pressure gradient the boundary layer works against. The velocities predicted by the CFD are smaller than those measured. We attribute this difference to the reattachment process.

The boundary layer profile at reattachment has a shape distinctive of reattaching turbulent shear layers. These layers are characterized by a linear increase in velocity from the wall out toward the boundary layer edge [18]. The figures show the inner structure of the recovering boundary layer developing just downstream of the reattachment point. The layer is accelerated through the inward entrainment of momentum from the outer region. Both experimental and CFD results show the sublayer developing with its characteristic thin region of steep velocity gradients. Moving further aft from the reattachment point, the boundary layer starts to show a typical turbulent boundary layer profile: The sublayer thickens, and the mixing layer structures in the outer region of the boundary layer spread and dissipate. At x/c=0.875, the inner region of the boundary layer appears to have recovered in the experiments and shows a profile similar to ZPG up to $y^+ \approx 50$. The outer region of the boundary layer—while showing its characteristic defect layer shape—still predicts low velocities and is yet to recovery fully.

The delayed postreattachment recovery of the boundary layers predicted by the CFD was also observed by So and Lai [19] for flow past a backward facing step. In their experiments, wall function based models produced better results in the recovery region than low Reynolds number turbulence models. This is not surprising because wall functions, which are based on local-equilibrium arguments, force the flow to asymptote to the log law of wall.

As a final note on the boundary layer profiles, Fig. 11 shows that the k-ω model predicts profiles that are slightly closer to the measured profiles than those predicted by the SST model. This is believed to be the consequence of the SST limiter on the eddy viscosity, which leads to less production of turbulent kinetic energy.

4.3.3 Pressure Distributions. The pressure coefficient plot for the flat plate at α=1 deg is presented in Fig. 12. In the experimental data, the pressure decreases downstream of the leading edge and reaches a minimum at $x/c \simeq 0.045$. The CFD results show a lower and flatter suction peak. They do not experience the gradual decrease in pressure over the forward half of the separation bubble that is seen in the experimental result because of the inability of the turbulence models to predict the correct transition location and resolve the secondary recirculation region. The experiments show a leading edge bubble that is shorter and fatter, indicating greater shear layer curvature. Within the leading edge bubble, the pressures, which are determined predominantly by the

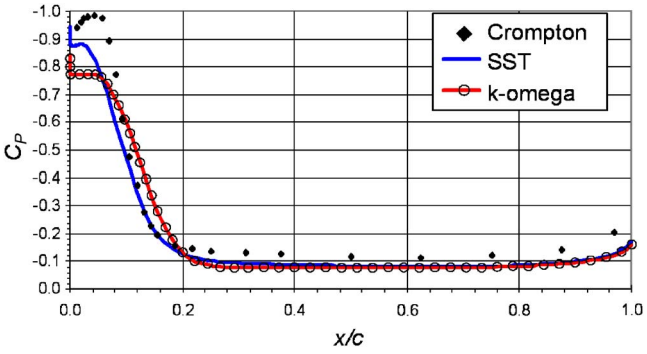

Fig. 12 Pressure coefficient plot (α=1 deg)

curvature of the outer shear layer, are lower. The shear layer is initially laminar and able to sustain a positive pressure gradient before transition. It is possible that background turbulence in the experiments may have helped to increase the curvature of the shear layer. Because the freestream turbulence intensity in the experiments was less than 0.25%, background turbulence was not likely to have caused an increase in shear layer curvature.

As shown in Fig. 12, the k-ω model predicts lower pressures than the SST model and the experimental data between x/c=0.1 and x/c=0.2. This is in agreement with the model overpredicting the length of the separation bubble.

When the C_P curves are normalized based on reattachment length, the pressure profiles compare well. The only significant differences are a larger suction at the leading edge in the experimental data and a particularly low suction peak predicted by the k-ω model. Downstream of reattachment, the pressure coefficients in the experimental results are slightly lower than in the CFD results. This is directly related to the greater velocities in both the leading edge bubble and the boundary layer in this flow region.

Table 2 Reattachment lengths for the flat plate at α=3 deg

	X_R
Crompton	0.47
SST	0.4374
k-ω	0.5096

4.4 Comparison at α=3 deg

4.4.1 Boundary Layer Profiles in the Leading Edge Bubble. The reattachment lengths for the α=3 deg case are presented in Table 2. The SST model underpredicts X_R by 6.4% and the k-ω model overpredicts X_R by 8.4%. As before, the chordwise positions are scaled by X_R.

The velocity profiles within the separation bubble are presented in Fig. 13. At the reattachment point (x/c=0.375), the velocities predicted by the CFD are much lower than the experimental data in both the outer and inner shear layers. As the shear layer curves down toward the wall, the velocities in the chordwise direction are damped inappropriately. We will address this point further in the next section.

The measurement station at x/c=0.25 is approximately mid length of the leading edge bubble. Here, the velocities are at their maximum, both at the outside edge of the shear layer and in the reversed flow region. In the inner shear layer, the maximum reversed velocity is $-0.393U_\infty$ for the experimental results, whereas the SST model predicts $-0.252U_\infty$ and the k-ω model predicts $-0.271U_\infty$. The reversed boundary layer is notably thicker in the experiments than in the CFD results. Moving toward the leading edge, we see that at x/c=0.125, the reversed flow weakens due to mass flow in the direction normal to the plate mostly. In the experiments, the presence of an adverse pressure gradient also contributes to this effect.

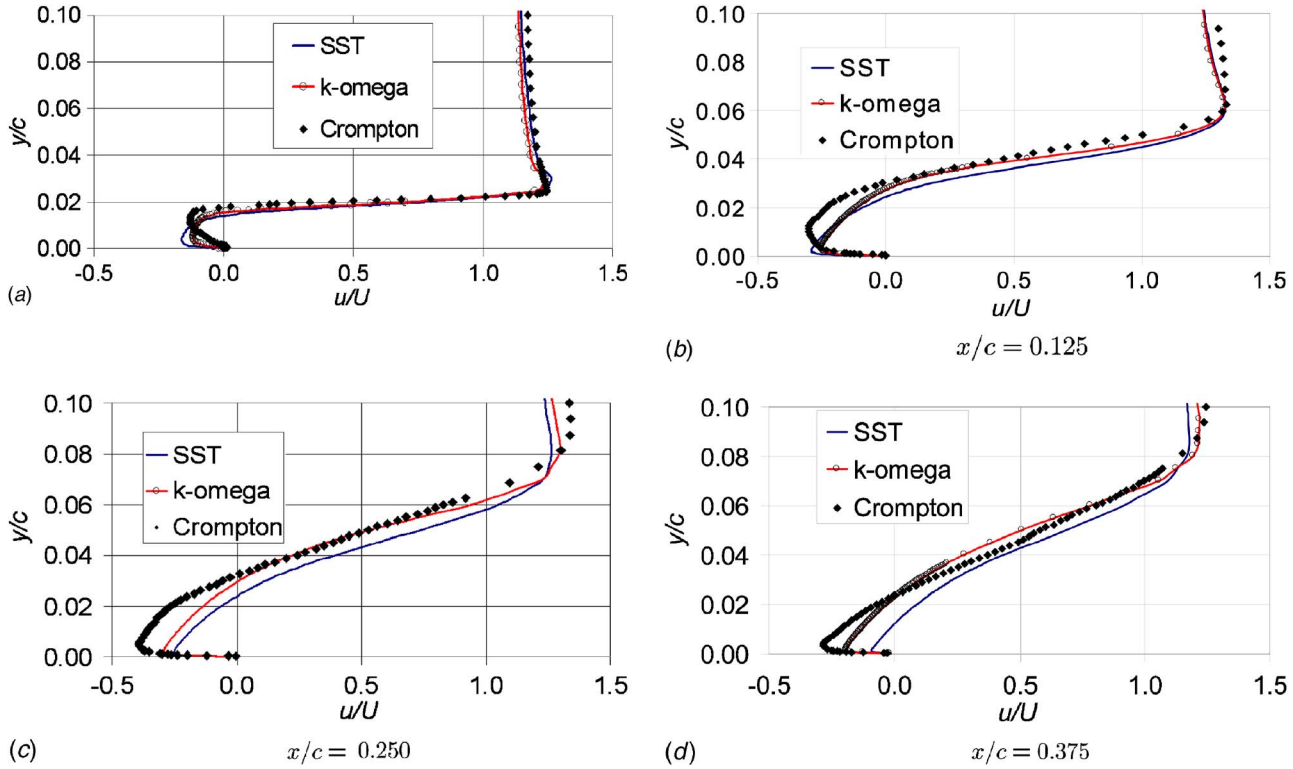

Fig. 13 Chordwise velocity profiles within the leading edge bubble (α=3 deg). (a) x/c=0.031, (b) x/c=0.125, (c) x/c=0.250, (d) x/c=0.375.

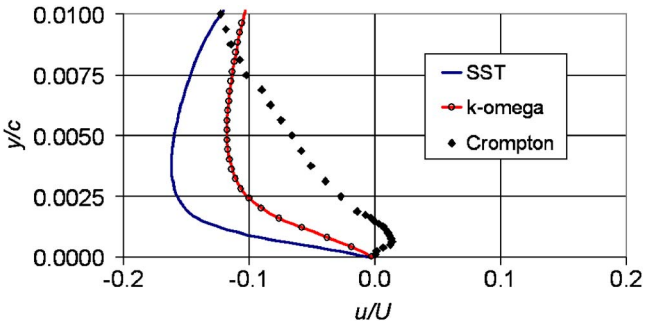

Fig. 14 Near-wall chordwise velocity profiles at $x/c=0.031$ ($\alpha=3$ deg)

At $x/c=0.031$, the secondary separation bubble presents itself in the experimental data, as shown in Fig. 14. The simulations do not show this feature, and the near-wall flow is reversed all the way to the leading edge.

4.4.2 Turbulent Kinetic Energy Profiles in the Leading Edge Bubble. In this section, we compare the turbulent kinetic energy profiles calculated by the CFD with the profiles from the experiments for the flow at $\alpha=3$ deg. Crompton's data were supplied in terms of u_{rms}, v_{rms}, and w_{rms}, where rms represents the root mean square of the velocity fluctuations. From these data, the turbulent kinetic energy was calculated as $k=1/2(\overline{u'u'}+\overline{v'v'}+\overline{w'w'})$, with the normal turbulent stresses given by $\overline{u'u'}=(u_{\text{rms}})$ [2]. The rms measurements cannot distinguish between turbulent fluctuations and the mean-flow unsteadiness that was observed in the shear layer. Periodicity in the rms velocities (indicating mean-flow unsteadiness) was observed as far back as $x/c=0.375$ for the $\alpha=3$ deg case. Therefore, the turbulent kinetic energy for the experimental data presented in Fig. 15 may be overestimated. Crompton reported that the vortical structures seen in the laminar shear layer were absorbed into the turbulent eddy spectrum downstream of the transition region. Therefore, the mean-flow kinetic energy associated with shear layer flapping is eventually converted into turbulent kinetic energy.

At $x/c=0.031$, the experimental turbulent kinetic energy profile shows two peaks. The first, and lower, peak is associated with the secondary separation bubble. At the outer edge of this bubble, a region of high mean shear exists, which increases production of turbulent kinetic energy. The second peak occurs at the point of inflection in the velocity profile in the outer shear layer where the mean shear is at its maximum. It is stronger than the first peak as it is driven by the large velocities around the leading edge of the plate. The maximum turbulent kinetic energy observed in the experiments is 2.5 times that predicted by the SST model and 4.0 times the maximum predicted by the k-ω model.

Naturally, care must be taken when comparing the three-dimensional experimental turbulence data to the two-dimensional simulation data. The contribution of the spanwise velocity fluctuations to the turbulent kinetic energy measured by Crompton is not negligible. However, because the turbulent energy originates from mean-flow shear, which is essentially two dimensional, we believe that the discrepancy between the simulations and the experiments cannot be fully explained by the difference in dimensionality. Our speculation is that two flow features that were not resolved by the CFD models are mostly responsible for the discrepancy: the unsteadiness at the leading edge, which feeds into the downstream turbulence spectrum, and the extra shear created by the secondary recirculation bubble.

The turbulent kinetic energy contours for the leading edge are illustrated in Fig. 16. Here, it can be seen that in the SST simulations the turbulent kinetic energy levels begin to be amplified slightly further upstream than they do for the k-ω model. While we have said that these turbulence models are not transition models, it is not true to say that they do not model transition at all. The simulations still pass from a region where the turbulent kinetic

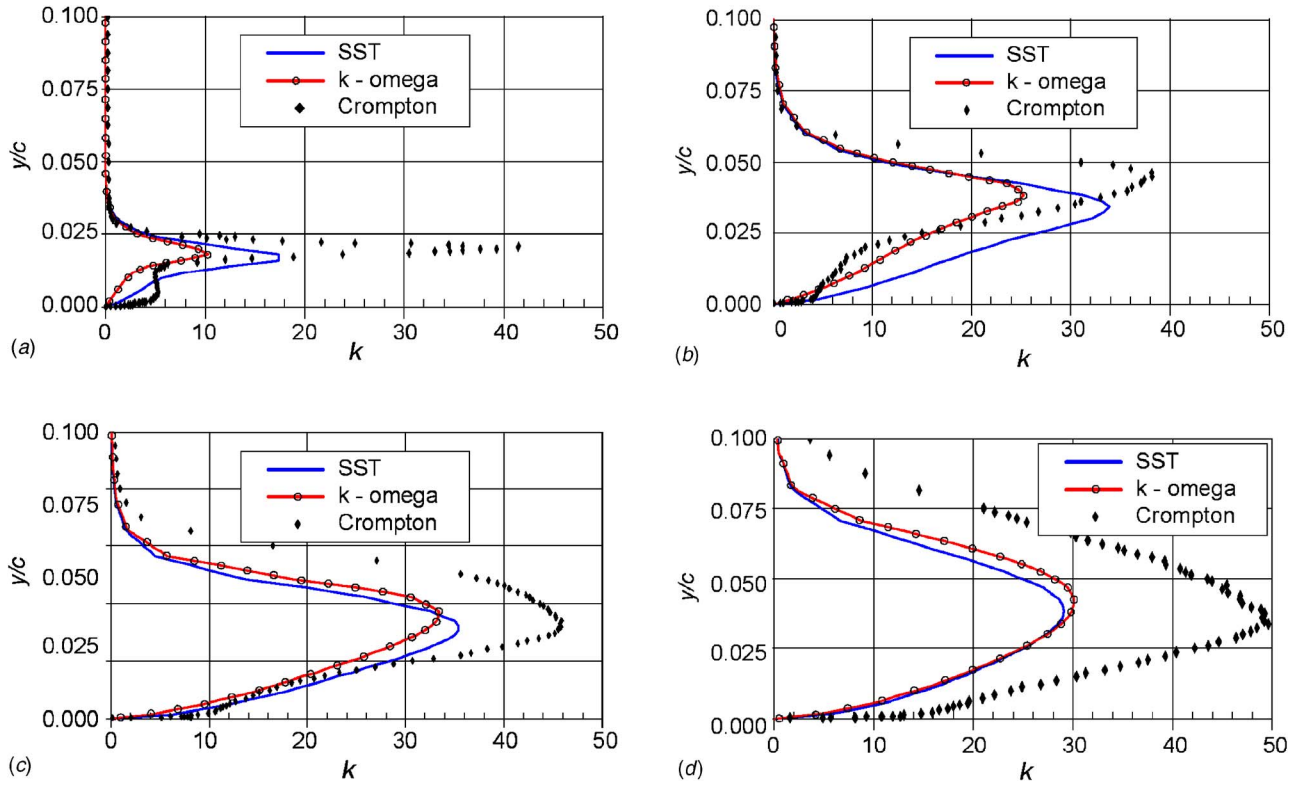

Fig. 15 Turbulent kinetic energy profiles within the leading edge bubble ($\alpha=3$ deg)

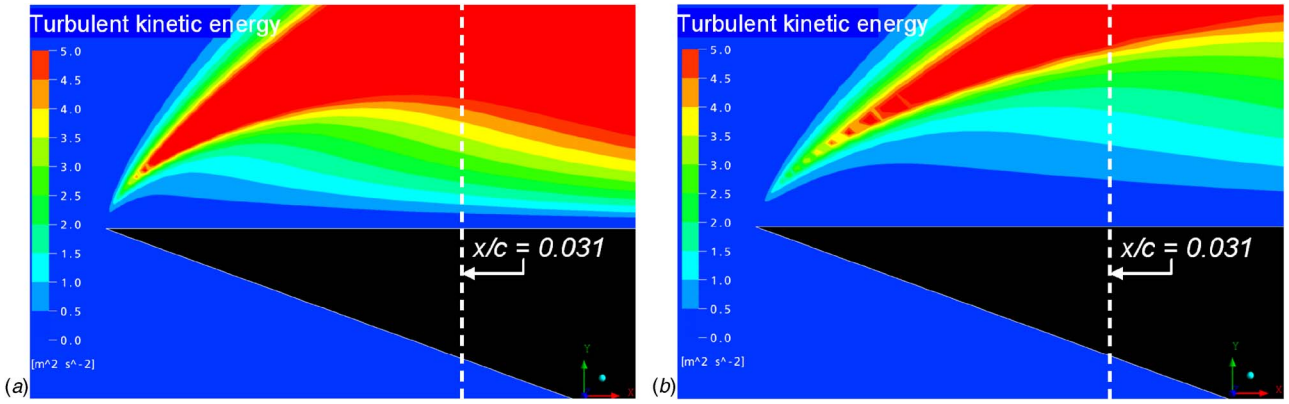

Fig. 16 Turbulent kinetic energy contours around the leading edge (α=3 deg). (a) SST, (b) k-ω.

energy is zero (i.e., a laminar region) through to a turbulent region where production terms in both the k and ω equations are positive, but they do not model the transition process appropriately. Typically, for transitional boundary layer flows, standard two-equation models will predict a transition to occur at a Reynolds number at least an order of magnitude too small [20]. Similarly, in this test case, transition occurs immediately after separation and much further upstream than the figure of 2.5%c reported by Crompton.

At x/c=0.125, the experiments give a peak magnitude of turbulent kinetic energy in the shear layer that is slightly lower than at the upstream station. This is due to the diminished effect of the secondary separation bubble, which extends only to x/c=0.045. This reduction in turbulent kinetic energy may also be associated with the diffusion of the unsteady structures that were observed in the shear layer near the leading edge. The turbulence models are in better agreement with the experiments than upstream with the SST model outperforming k-ω. In both the CFD and the experimental results, the peak in turbulent kinetic energy has widened due to the thickening of the shear layer. Near the wall, the experimental results show lower levels of turbulent kinetic energy than the CFD, which is a result of relaminarization of the reversed boundary layer.

Between x/c=0.125 and x/c=0.25, the experimental results indicate that the kinetic energy in the shear layer is still increasing and that the maximum entrainment rate has not yet been reached. The shear layer predicted by the SST model reaches a local equilibrium prematurely because the SST limiter reduces the amount of turbulent shear stress and hence the production of turbulent kinetic energy.

Between x/c=0.250 and x/c=0.375, both the SST and k-ω models predict a decrease in turbulent kinetic energy, whereas in the experimental results k continues to increase. In this region, the shear layer curves back toward the wall and decelerates as it approaches reattachment. The experimental results show a drop in vertical velocity fluctuations (v'). This energy is mostly converted to transverse (w') and streamwise (u') velocity fluctuations, and thus the kinetic energy levels are retained. The SST and k-ω turbulence models cannot emulate this transfer of energy from the vertical to transverse and streamwise fluctuations because they assume isotropy of the Reynolds stress tensor. In order to model this process, a more advanced anisotropic turbulence model is required, such as an algebraic stress model or a second-order closure model.

At x/c=0.375, both the SST model and the k-ω model predict peaks in turbulent kinetic energy that are approximately 1.7 times smaller than in the experimental results. In the experimental results, the kinetic energy peak is wider, which indicates that the shear layer thickness is underpredicted by the CFD.

4.4.3 Downstream of Reattachment. For the α=3 deg case, the downstream velocity profiles are quite similar in shape to those found in the α=1 deg case. Again, in this region, the velocities predicted by the CFD are lower than those measured in the experiments. It is likely that in the experiments the outer turbulent structures, which originate in the shear layer of the leading edge bubble, feed energy into the inner region and in this way accelerate the development of turbulence. Without these increased levels of turbulent kinetic energy, the recovery of the boundary occurs over a larger downstream distance in the CFD. It is hoped that future LES simulations will be able to help us to improve our understanding of this apparent slow postreattachment recovery of the two-equation turbulence models.

In the recovery region, the k-ω model predicts greater turbulent kinetic energy compared with SST. Consequently, the k-ω model predicts slightly steeper near-wall velocity gradients, and the turbulent boundary layer is able to recover more rapidly. The lower values of turbulent kinetic energy in the SST results are due to the SST limiter, which becomes active in regions of large mean strain.

Directly behind the square trailing edge, a small pair of steady vortices appear in the CFD results. A steady wake forms downstream. Unfortunately, the experimental data do not include flow measurements downstream of the plate.

5 Summary

5.1 Experiments Versus SST and k-ω Simulations. The experimental results show greater growth and curvature of the outer shear layer of the leading edge bubble. This is due to several phenomena that are not adequately captured by the SST and k-ω turbulence models: Firstly, there is increased entrainment in the experimental results at the leading edge due to unsteady shear layer flapping. Also, transport and production of turbulent kinetic energy dominate turbulent kinetic energy dissipation, and k continues to increase along the length of the shear layer in the experiments. The lower shear layer growth predicted by the CFD causes reattachment to be delayed and the pressure coefficient to be overpredicted within the leading edge bubble.

The reversed flow in the leading edge bubble is subject to a favorable pressure gradient, which causes relaminarization, an effect which is not captured by the turbulence models because they are designed for fully turbulent flows and are incapable of modeling transitional effects. Consequently, the models also fail to predict the secondary bubble near the leading edge. The omission of the secondary bubble in the CFD results is not believed to be an artifact of the numerics since the solutions showed excellent grid convergence and the secondary bubble was not present in the fine grid simulations.

Approaching the reattachment point, both turbulence models artificially damp turbulent kinetic energy due to the presence of the wall. In the experiments, the turbulent fluctuations normal to

the wall were damped; however, the energy from this was fed into the spanwise and chordwise turbulence. The k-ω and SST models use an isotropic formulation of the Reynolds stress tensor and are thus unable to model this anisotropic effect.

Downstream of reattachment, the CFD profiles recover toward turbulent equilibrium slowly compared with the experiments. In the observed recovering boundary layer, the eddies in the outer region of the near wall originate in the separated shear layer, whereas the scales in the inner region are associated with the development of the new boundary layer. The two-equation turbulence models cannot be expected to emulate this complicated recovery process involving an irregular eddy spectrum. Also, the anisotropic effects that occur as the shear layer approaches reattachment, which leads to transfer of turbulent kinetic energy from the normal to the transverse and streamwise velocity fluctuations, cannot be captured by the turbulence models. The models instead damp the turbulent kinetic energy associated with the velocity fluctuations normal to the plate near the reattachment point. The CFD predicts a slower recovery of the boundary layer downstream of reattachment.

5.2 SST Versus k-ω. The SST model captures the leading edge bubble more accurately than the k-ω model. It predicts greater turbulent kinetic energy levels near the leading edge and therefore predicts greater shear layer growth. As a result, its predictions of the reattachment lengths are in closer agreement with the observed lengths (within 7% for both angles of attack that were investigated (α=1 deg and α=3 deg)), and the pressure coefficient in the vicinity of the leading edge bubble is more accurate. The shear layer predicted by the SST model has more curvature and bends back toward the plate earlier than the layer predicted by the k-ω model. However, the SST model returns lower turbulent kinetic energy values in the rear half of the leading edge bubble. This is due to the SST limiter. As a consequence, the SST model produces lower velocities in both the outer and inner shear layers compared with both the k-ω model and the experimental data.

Downstream of reattachment, the k-ω model predicts a more rapid boundary layer recovery than the SST model, but the recovery is still slower than observed in the experiments. The differences between the velocity profiles predicted by the two turbulence models are small and are a consequence of the SST limiter.

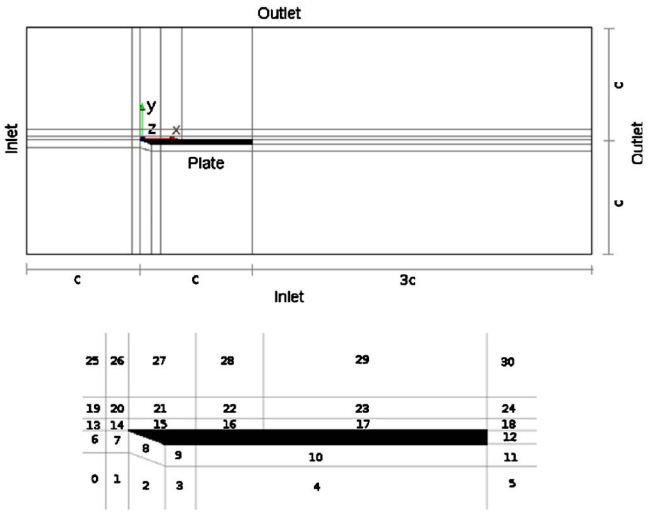

Fig. 17 Thin flat plate geometry and auxiliary block numbers

6 Discussion and Conclusions

The flow past the flat plate at shallow incidence is a complex and challenging assignment for two-equation turbulence models.

The overall flow topology of the leading edge bubble was predicted with reasonable accuracy by both the k-ω and SST turbulence models despite the fact that both turbulence models did not capture the secondary bubble. Both the k-ω and SST models underpredicted the production of turbulent kinetic energy within the leading edge bubble, which resulted in lower velocities in both the outer and inner shear layers.

A proper prediction of the recovering boundary layer downstream is particularly difficult for such turbulence models. We expect that CFD boundary layer profiles will be more susceptible to flow separation when an adverse pressure gradient is present, as is the case, for example, for curved sails. A question certainly remains over how the unsteady structures in the turbulent shear layer interact with the turbulence within the shear layer and how they affect the downstream behavior of the flow. These structures are damped by turbulence models because of the high eddy viscosities around stagnation and the leading edge. LES results would be useful here as a tool to aid the understanding of the transient behavior.

For the validation of sail flow simulations, several results from this chapter are encouraging. Firstly, the overall flow topology of the leading edge bubble and recovering boundary layer is predicted reasonably well, and the pressure coefficient plots are close to the experimental data, especially for the SST model. Secondly, despite using turbulence models that assume fully turbulent flow, the leading edge bubble was adequately captured. This is largely because the leading edge bubble involves little laminar flow, with the shear layer undergoing transition within the first 2.5% of the length of the plate. Therefore, turbulence models that do not account for transition can be much more suitably applied to the thin

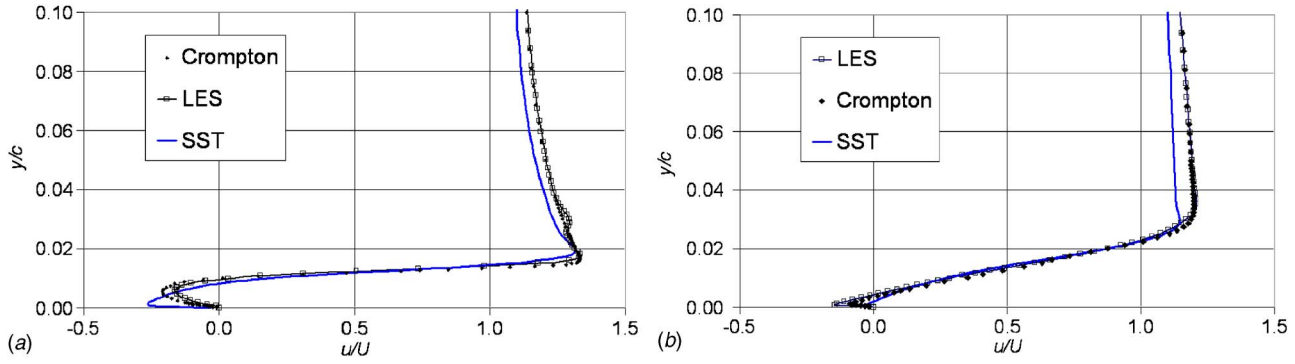

Fig. 18 LES chordwise velocity profiles within the leading edge bubble (α=1 deg). (a) x/c=0.031, (b) x/c=0.125.

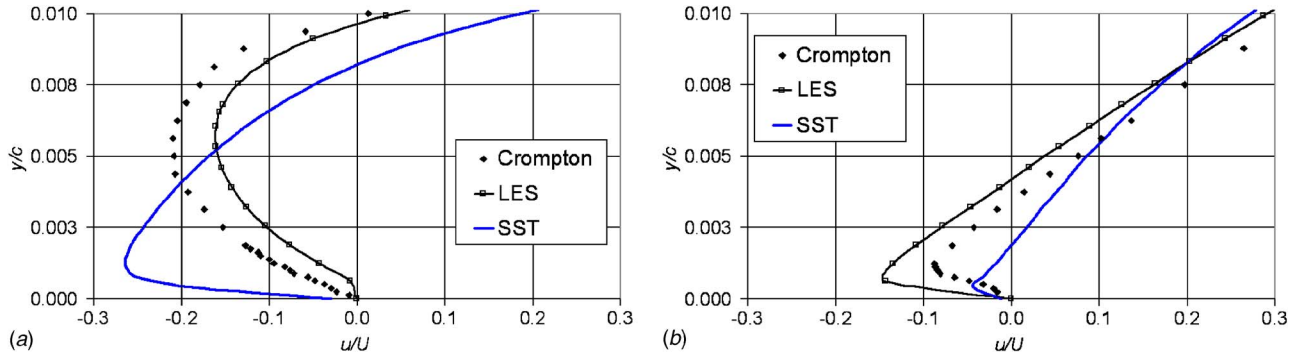

Fig. 19 LES near-wall chordwise velocity profiles within the leading edge bubble (α=1 deg). (a) x/c=0.031, (b) x/c=0.125.

airfoil bubble than the short bubble where extensive regions of laminar flow exist, both upstream of the bubble and within the separated region itself.

A correct prediction of the pressure distribution is the most important criterion for evaluating turbulence models for sail flow simulations since almost all of the lift and drag is generated from the pressure forces. Based on this method of evaluation, the SST model is preferred over the k-ω model. Considering the complexity of this flow and just how different it is to flows that modelers usually investigate and tune in their models, the results are actually quite pleasing.

6.1 Preliminary Results From LES Study. We present preliminary LES results for the plate at 1 deg angle obtained using the opensource framework OPENFOAM [21] (see also Ref. [22]). OPENFOAM's solvers are based on a cell-centered finite volume method and employ the PISO algorithm [23] with a second order time discretization. We selected the one-equation subgrid model of Horiuti [24] for its ability to deal with nonequilibrium conditions.

Figure 17 shows the computational domain and its division in subdomains used to aid the distribution of the mesh elements, and also describes the boundary conditions. The mesh has a total of 837,984 cells. We use 32 cells in the z direction, which spans 1/4th of the chord. The average y^+ value is 3.9 on the top surface, which is too high for boundary layer flows; however, more focus was placed on achieving sufficient grid density in the leading edge bubble and, in particular, the outer shear layer. To reduce computational costs, the computational domain was reduced and the grid stretched in regions away from the plate. To avoid numerical instabilities caused by grid stretching, the computational domain is partitioned into two regions. The first, which includes the flat plate and surrounding areas (regions 7–12, 14–18, and 20–24 in Fig. 17) with turbulent activity, has a fine, high-quality grid, and is discretized using a nondissipative scheme so that turbulent structures are well represented. Grid stretching is confined to the second, outer area where a dissipative scheme guarantees numerical stability.

The LES results are encouraging. In regions with an adequate grid density, the LES does a better job than the two-equation models at capturing the physics. For example, the maximum velocities of the outer and inner shear layers are computed more accurately. Also, the relaminarization of the leading edge bubble and the secondary bubble are captured (see Figs. 18 and 19). In the recovery region (see Fig. 20), the grid spacing used near the wall is inadequate. As a consequence, the recovery region is resolved no more accurately than with the two-equation models. Further results are presented in the thesis of Sampaio [25].

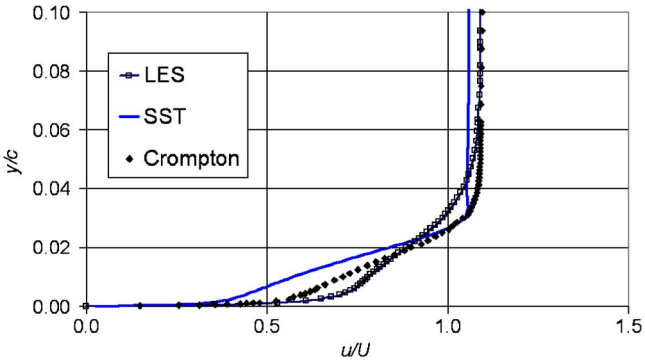

Fig. 20 LES boundary layer profile just downstream of reattachment (x/c=0.25)

References

[1] Crompton, M. J., 2001, "The Thin Aerofoil Leading Edge Bubble," Ph.D. thesis, University of Bristol.

[2] Bardina, J. E., Huang, P. G., and Coakley, T. J., 1997, "Turbulence Modeling Validation, Testing and Development," NASA, Technical Report No. 110446.

[3] Collie, S., and Gerritsen, M., 2006, "The Challenging Turbulent Flows Past Downwind Yacht Sails and Practical Application of CFD to Them," *Second High Performance Yacht Design Conference*, Auckland.

[4] Gault, D. E., 1957, "An Investigation at Low Speed of the Flow Over a Simulated Flat Plate at Small Angles of Attack Using Pitot Static and Hot-Wire Probes," NACA, Technical Report No. TN-3876.

[5] Driver, D. M., Seegmiller, H. L., and Marvin, J. G., 1987, "Time-Dependent Behavior of a Reattaching Shear Layer," AIAA J., **25**(7), pp. 914–919.

[6] Driver, D. M., and Seegmiller, H. L., 1985, "Features of a Reattaching Turbulent Shear Layer in Divergent Channel Flow," AIAA J., **23**(2), pp. 163–171.

[7] Menter, F. R., 1992, "Improved Two-Equation k-ω Turbulence Models For Aerodynamic Flows," NASA, Technical Report No. TM-103975.

[8] Crabtree, L. F., 1957, "The Formation of Regions of Separated Flow on Wing Surfaces," Aeronautical Research Council, London, Technical Report No. R&M-3122.

[9] Newman, B. G., and Tse, M.-C., 1992, "Incompressible Flow Past a Flat Plate Aerofoil With Leading Edge Separation Bubble," Aeronaut. J., **96**, pp. 57–64.

[10] Cherry, N. J., Hiller, R., and Latour, M. E. M. P., 1983, "The Unsteady Structure of Two-Dimensional Separated-and-Reattaching Flows," J. Wind. Eng. Ind. Aerodyn., **11**, pp. 95–105.

[11] Kiya, M., and Sasaki, K., 1983, "Structure of a Turbulent Separation Bubble," J. Fluid Mech., **137**, pp. 83–112.

[12] CFX-International 2003, CFX-5 Solver and Solver Manager Version 5.6, CFX-International.

[13] Raw, M., 1996, "Robustness of Coupled Algebraic Multigrid for the Navier-Stokes Equations," *34th Aerospace Sciences Meeting and Exhibit*, Reno, NV, AIAA Paper No. 96-0297.

[14] Menter, F. R., 1994, "Two-Equation Eddy-Viscosity Turbulence Models For Engineering Applications," AIAA J., **32**(8), pp. 1598–1605.

[15] Wilcox, D. C., 1988, "Reassessment of the Scale-Determining Equation for Advanced Turbulence Models," AIAA J., **26**(11), pp. 1299–1310.

[16] ICEM-CFD-Engineering, "ICEM HEXA 4.2," http://www.icemcfd.com/

[17] Österlund, J., 1999, "Experimental Studies of Zero Pressure-Gradient Turbulent Boundary Layer Flow," Ph.D. thesis, Kungl Tekniska Högskolan.

[18] Horton, H. R., 1969, "A Semi-Empirical Theory for the Growth and Bursting of Laminar Separation Bubbles," Aeronautical Research Council, London, Technical Report No. ARC CP-1073.

[19] So, R. M. C., and Lai, Y. G., 1988, "Low-Reynolds-Number Modeling of Flows Over a Backward Facing Step," ZAMP, **39**, pp. 13–27.
[20] Wilcox, D. C., 1998, *Turbulence Modeling for CFD*, 2nd ed., Griffin, California.
[21] Weller, H., Tabor, G., Jasak, H., and Fureby, C., 1998, "A Tensorial Approach to Computational Continuum Mechanics Using Object Orientated Techniques," Comput. Phys., **12**(6), pp. 620–631.
[22] Sampaio, L. E. B., Nieckele, A. O., Gerritsen, M., and Collie, S., 2006, "Numerical Simulations of the Long Recirculation Bubbles Formed in Thin Flat Plates at Shallow Incidence," *Proceedings of the EPTT 2006, Escola de Primavera de Transicao e Turbulencia, ABCM*, Brazil Society of Mechanical Sciences and Engineering—ABCM, Rio De Janeiro, RJ, Brazil.
[23] Issa, R., 1985, "Solution of the Implicit Discretized Fluid Flow Equations by Operator-Splitting," J. Comput. Phys., **62**, pp. 40–65.
[24] Horiuti, K., 1985, "Large Eddy Simulation of Turbulent Channel Flow by One-Equation Modeling," J. Phys. Soc. Jpn., **54**(8), pp. 2855–2865.
[25] Sampaio, L. E. B., 2006, "Large Eddy Simulations of the Thin Plate Separation Bubble at Shallow Incidence," Ph.D. thesis, Department of Mechanical Engineering, Pontifícia Universidade Católica do Rio de Janeiro, RJ, Brasil, in Portuguese.